

Supporting Information

A low-temperature co-precipitation approach to synthesize fluoride phosphors $K_2MF_6:Mn^{4+}$ (M = Ge, Si) for white LED applications

Ling-Ling Wei,^a Chun Che Lin,^b Mu-Huai Fang,^b Mikhail G. Brik,^c Shu-Fen Hu,^d
Huan Jiao^{*a} and Ru-Shi Liu^{*be}

^aSchool of Chemistry and Chemical Engineering, Shaanxi Normal University, Xi'an
710062 Shaanxi, P.R. China

^bDepartment of Chemistry, National Taiwan University, Taipei 106, Taiwan

^cCollege of Mathematics and Physics, Chongqing University of Posts and
Telecommunications, Chongqing 400065, P.R. China and Institute of Physics,
University of Tartu, Ravila 14C, Tartu, 50411, Estonia

^dDepartment of Physics, National Taiwan Normal University, Taipei 116, Taiwan

^eDepartment of Mechanical Engineering and Graduate Institute of Manufacturing
Technology, National Taipei University of Technology, Taipei 106, Taiwan

Theoretical calculations

(I) Crystal field calculations of the Mn^{4+} energy levels in K_2SiF_6 and K_2GeF_6

The energy levels of the Mn^{4+} ions in K_2SiF_6 and K_2GeF_6 were obtained by diagonalizing the following crystal field Hamiltonian:¹

$$H = \sum_{p=2,4} \sum_{k=-p}^p B_p^k O_p^k . \quad (1)$$

where O_p^k are the linear combinations of the spherical operators acting on the angular parts of the wave functions [exact definition of the operators used in the exchange charge model (ECM) are given in Reference (1) and (2)] of the impurity ions. B_p^k stands for the crystal field parameters (CFPs), which can be calculated using crystal structure data without making any *a priori* assumption or approximation of the site symmetry at the impurity ion's position. The Hamiltonian (discussed in the manuscript) can be diagonalized based on set determined by all wave functions of the LS terms (which arose given the Coulomb interaction between electrons of an impurity ion) of the free ion.¹ The ECM allows the representation of the CFPs as a sum of two terms:

$$B_p^k = B_{p,q}^k + B_{p,s}^k , \quad (2)$$

with

$$B_{p,q}^k = -K_p^k e^2 \langle r^p \rangle \sum_i q_i \frac{V_p^k(\theta_i, \varphi_i)}{R_i^{p+1}} , \quad (3)$$

and

$$B_{p,S}^k = K_p^k e^2 \frac{2(2p+1)}{5} \sum_i \left(G_s S(s)_i^2 + G_\sigma S(\sigma)_i^2 + \gamma_p G_\pi S(\pi)_i^2 \right) \frac{V_p^k(\theta_i, \varphi_i)}{R_i} \quad (4)$$

The first term $B_{p,q}^k$ is the point charge contribution to the CFPs. This phenomenon is due to the Coulomb interaction between the impurity ion and the lattice ions enumerated by index i with charges q_i and spherical coordinates R_i, θ_i, φ_i (with the reference system focused on the impurity ion itself). At this point, the impurity ion and ligands are treated as the point charges. The averaged values $\langle r^p \rangle$, where r is the radial coordinate of the d electrons of the optical center (also known as the moments of the 3d electron density), can be easily calculated numerically using the radial parts of the wave functions of the corresponding ion. The numerical factors K_p^k, γ_p , the expressions for the polynomials V_p^k , and the definitions of the operators O_p^k are all given in Reference (2), and thus are not shown here for brevity. The second term of Eq. (2) $B_{p,S}^k$ is proportional to the overlap between the wave functions of the impurity ion and ligands to include the covalent and exchange effects. At this point, the impurity ion and ligands are treated quantum-mechanically, clearly distinguishing between different orbitals of the ions involved into the chemical bond formation. The $S(s), S(\sigma), S(\pi)$ terms denote the overlapping integrals between the d -functions of the impurity ion and p - and s -functions of the ligands:

$$S(s) = \langle d0|s0 \rangle, S(\sigma) = \langle d0|p0 \rangle, S(\pi) = \langle d1|p1 \rangle. \quad (5)$$

The G_s, G_σ, G_π coefficients stand for the dimensionless adjustable parameters of

the ECM, whose values are determined from the positions of the lowest in the three energy absorption bands in the experimental spectrum. They are considered equal, such that $G_s = G_\sigma = G_\pi = G$ estimated from one absorption band only (the lowest in energy). The summation in Eq. (4) includes only the nearest neighbors of an impurity ion (i.e. six ligands in the case of an octahedral impurity center) because of the overlap in the ions from the second, third, and so on; thus, coordination spheres can be safely disregarded. The ECM uses a small number of fitting parameters, which is one of the strongest points of the model. It also facilitates the calculation of the CFPs and energy levels of impurities in crystals without invoking any assumptions about the impurity center symmetry. This phenomenon is also very important for a consistent analysis of the low-symmetry crystal field effects and comparative studies of isostructural/isoelectronic systems. The ECM has been successfully used to calculate the energy levels of rare earth ions^{1, 3, 4} and transition metal ions.^{2, 5-7}

Using the experimental structural data, two large clusters consisting of 73261 ions in the case of K_2GeF_6 and 56630 ions in K_2SiF_6 were built. The crystal lattice ions at a distance up to 108 Å from the site of the impurity ion were considered. These big clusters eliminated all possible problems of the crystal lattice sums convergence. Applications of Eqs. (1) - (4) resulted in the values of the CFPs listed in Table S4. Table S4 shows that the second contribution $B_{p,S}^k$ to the CFPs values is vital, being

nine times greater than the $B_{p,q}^k$ in the case of B_4^3 . Next, the CF Hamiltonian with the CFPs from Table S4 was diagonalized in the space spanned by all wave functions of 8 LS terms of the d^3 electron configuration of the Mn^{4+} ions. The energy levels were calculated and are given in Table 1 and presented in Figure 3a.

(II) *ab initio* calculations of the structural, electronic, and optical properties of neat K_2SiF_6 and K_2GeF_6 single crystals

Ab initio calculations became an indispensable tool for assessing perspectives of applications of materials and their limitations. In the present article, the cambridge serial total energy package (CASTEP) module⁸ of Materials Studio package were employed. The exchange-correlation effects were considered in the frameworks of the generalized gradient approximation (GGA) with the Perdew-Burke-Ernzerhof⁹ and the local density approximation (LDA) with the Ceperley-Alder-Perdew-Zunger (CA-PZ) functional^{10, 11}. In case of K_2GeF_6 , the electronic configurations were $3s^23p^64s^1$ for K, $4s^24p^2$ for Ge, and $2s^22p^5$ for F. The convergence parameters were: 5×10^{-6} eV/atom for energy, 0.01 eV/Å for maximal force, 0.02 GPa for maximal stress and 5×10^{-4} Å for a maximal displacement. The plane-wave basis set cut off energy was set to 370 eV, and the Monkhorst-Pack k-points mesh was $8 \times 8 \times 8$. The electronic, optical and elastic properties of K_2SiF_6 were calculated in Reference (12), and are presented here for comparison with those of K_2GeF_6 . The calculated structural data

(Table S5) for both K_2GeF_6 and K_2SiF_6 agree with the experimental data (Table S2 and S3). The GGA/LDA-calculated data are slightly over-/underestimated compared with the experimental data.

Table S1. Examples of white LEDs that incorporate Blue-LEDs excitable red phosphors.

Red Phosphor	Chemical	Emission Characteristics			
	Composition	Width	External QE (%)	Thermal stability (% (%, 150°C))	drawback
	$K_2GeF_6:Mn^{4+}$	narrow	54	95	moisture-sensitive
	$(Ca,Sr)_2Si_5N_8:Eu$	Broad	71	74	re-absorption more red
	$CaAlSiN_3:Eu$	Broad	65	82	expensive

Table S2. Crystallographic parameters from X-ray Rietveld refinements for $\text{K}_2\text{Ge}_{0.95}\text{F}_6:\text{Mn}^{4+}_{0.05}$.

Atoms	x	y	z	Frac	U_{iso}
Ge	0.0000(0)	0.0000(0)	0.0000(0)	0.95	0.0115(2)
Mn	0.0000(0)	0.0000(0)	0.0000(0)	0.05	0.0092(3)
K	0.3333(0)	0.6667(0)	0.6972(2)	1.00	0.0184(1)
F	0.1495(1)	0.8505(3)	0.2194(0)	1.00	0.0197(1)
Space group	<i>P</i> 4mm				
Cell	$a = b = 5.63171(6) \text{ \AA}$ $c = 4.66751(6) \text{ \AA}$				
Parameters	$\alpha = \beta = 90^\circ$ $\gamma = 120^\circ$ $V = 128.2027(20) \text{ \AA}^3$				
Reliability	$\chi^2 = 2.237$				
Factors	$R_{\text{wp}} = 5.45\%$ $R_{\text{p}} = 3.09\%$				

Table S3. Crystallographic parameters from X-ray Rietveld refinements for $\text{K}_2\text{Si}_{0.95}\text{F}_6:\text{Mn}^{4+}_{0.05}$.

Atoms	x	y	z	Frac	U_{iso}
Si	0.0000(0)	0.0000(0)	0.0000(0)	0.95	0.0065(1)
Mn	0.0000(0)	0.0000(0)	0.0000(0)	0.05	0.0048(0)
K	0.2500(0)	0.2500(0)	0.2500(0)	1.00	0.0039(2)
F	0.2056(2)	0.0000(0)	0.0000(0)	1.00	0.0090(1)
Space group	<i>Fm3m</i>				
Cell	$a = b = c = 8.13107(7) \text{ \AA}$		$\alpha = \beta = \gamma = 90^\circ$		
Parameters	$V = 537.579(8) \text{ \AA}^3$				
Reliability	$\chi^2 = 1.538$				
Factors	$R_{\text{wp}} = 8.79\%$		$R_{\text{p}} = 5.88\%$		

Table S4. Calculated values of CFPs (Stevens normalization, in cm^{-1}). The ECM parameter $G = 7.770$ for K_2GeF_6 and 4.714 for K_2SiF_6 .

CFP	$B_{p,q}^k$	$B_{p,S}^k$	Total value $B_{p,q}^k + B_{p,S}^k$
K_2GeF_6			
B_2^0	344.9	-152.9	192.0
B_4^0	-348.1	-3380.5	-3728.6
B_4^3	10305.6	96475.2	106780.8
K_2SiF_6			
B_4^0	776.4	4992.5	5768.9
B_4^4	3881.8	24962.7	28844.5

Table S5. Calculated lattice parameters and fractional atomic coordinates for K_2GeF_6 and K_2SiF_6 .

K_2GeF_6			K_2SiF_6				
	Exp.	GGA	LDA		Exp.	GGA	LDA
$a, \text{\AA}$	5.63171	5.7464	5.4167	$a, \text{\AA}$	8.13107	8.1684	7.7026
$c, \text{\AA}$	4.66751	4.7999	4.4380				
	0.3333	0.3333	0.3333		0.2500	0.2500	0.2500
K	0.6667	0.6667	0.6667	K	0.2500	0.2500	0.2500
	0.6972	0.7020	0.6989		0.2500	0.2500	0.2500
	0.0000	0.0000	0.0000		0.0000	0.0000	0.0000
Ge	0.0000	0.0000	0.0000	Si	0.0000	0.0000	0.0000
	0.0000	0.0000	0.0000		0.0000	0.0000	0.0000
	0.1495	0.1532	0.1572		0.2056	0.2085	0.2175
F	0.8505	0.8468	0.8428	F	0.0000	0.0000	0.0000
	0.2194	0.2158	0.2242		0.0000	0.0000	0.0000

Table S6. Calculated effective Mulliken charges (GGA/LDA) for K_2GeF_6 and K_2SiF_6 .

K_2GeF_6	Charge	K_2SiF_6	Charge
K	0.81/0.72	K	0.97/1.02
Ge	2.02/2.28	Si	2.11/2.05
F	-0.60/-0.62	F	-0.67/-0.68

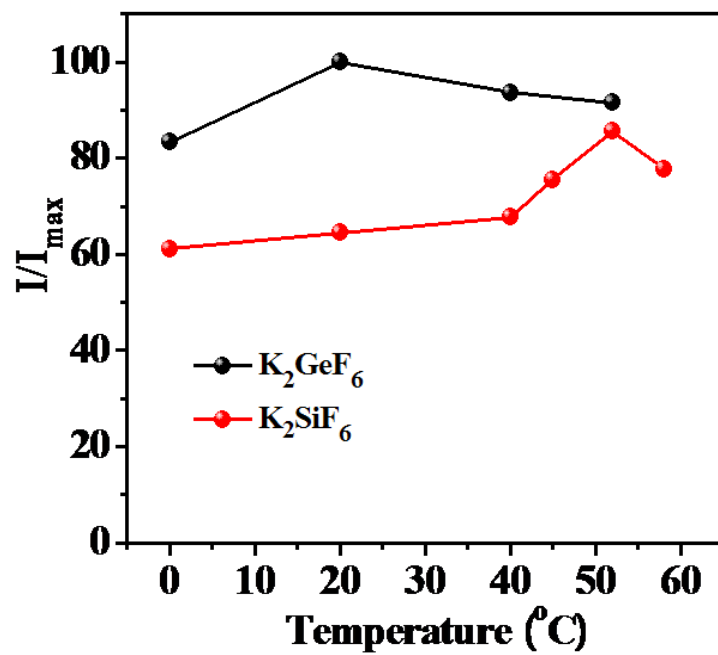


Figure S1. Comparison between the luminescence intensities of $K_2GeF_6:Mn^{4+}$ and $K_2SiF_6:Mn^{4+}$ red phosphors as a function of synthesizing temperature, with respect to the intensity of $K_2GeF_6:Mn^{4+}$ synthesized at 25 °C.

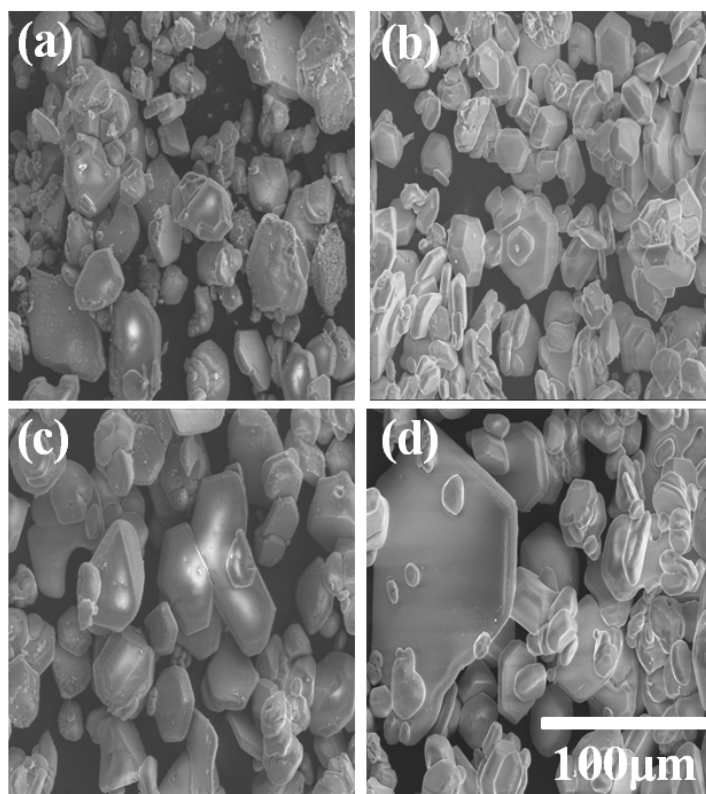


Figure S2. SEM images of $\text{K}_2\text{GeF}_6:\text{Mn}^{4+}$ powders synthesized at different temperatures: (a) 0 °C, (b) 25 °C, (c) 40 °C, and (d) 52 °C.

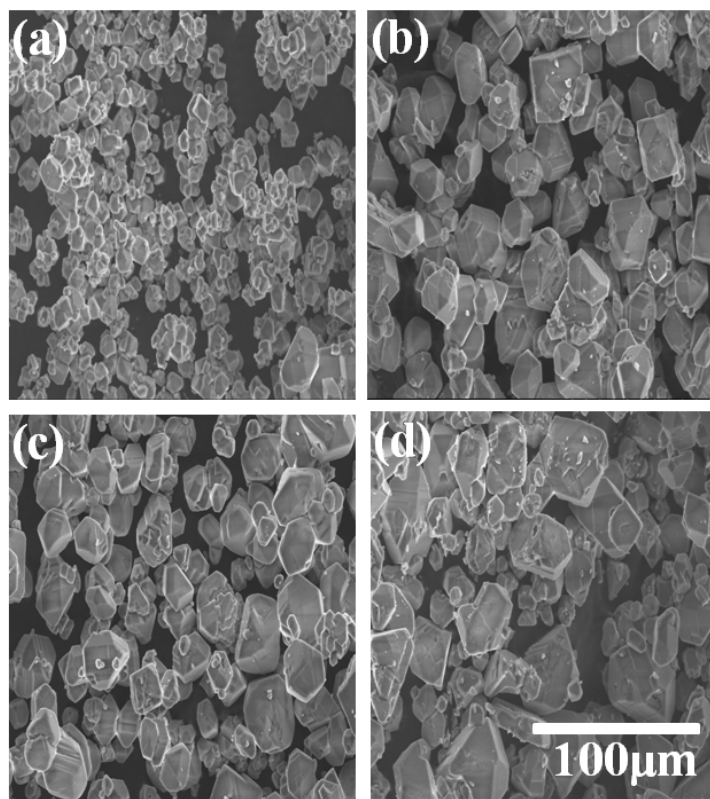


Figure S3. SEM images of $\text{K}_2\text{SiF}_6:\text{Mn}^{4+}$ powders synthesized at different temperatures:

(a) 0 °C, (b) 40 °C, (c) 52°C, and (d) 60°C.

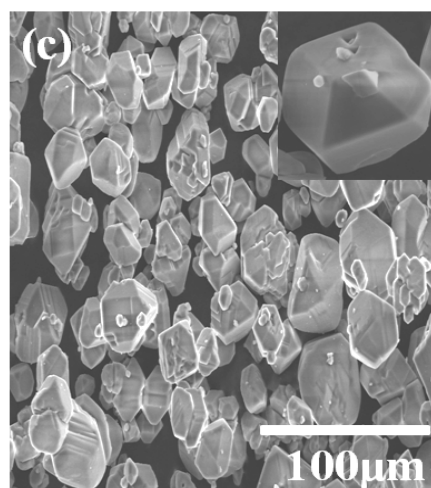
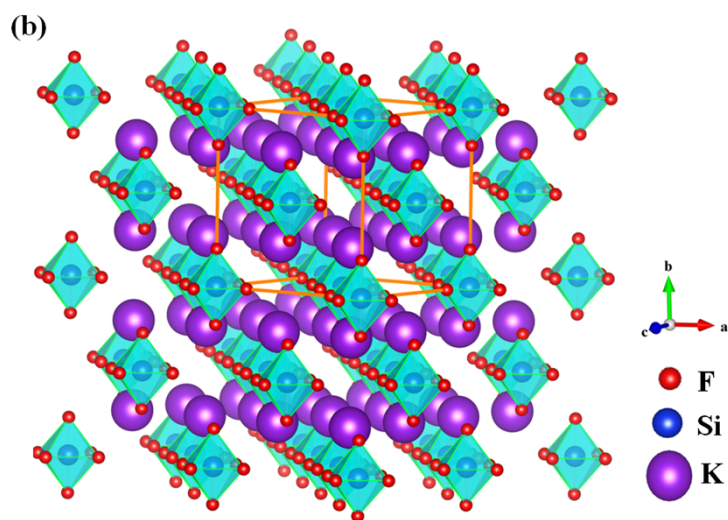
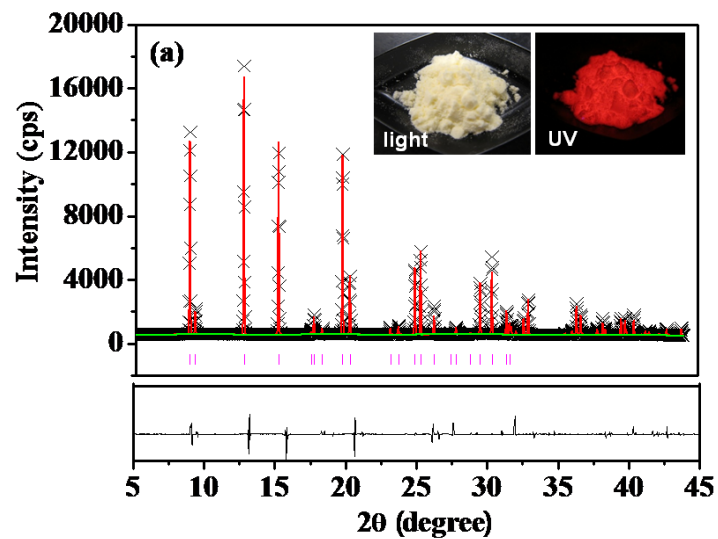


Figure S4. (a) X-ray Rietveld refinements of $\text{K}_2\text{SiF}_6:\text{Mn}^{4+}$ powders. (b) Crystal structure of $2 \times 2 \times 2$ unit cells. (c) SEM image of $\text{K}_2\text{SiF}_6:\text{Mn}^{4+}$ synthesized at 52°C .

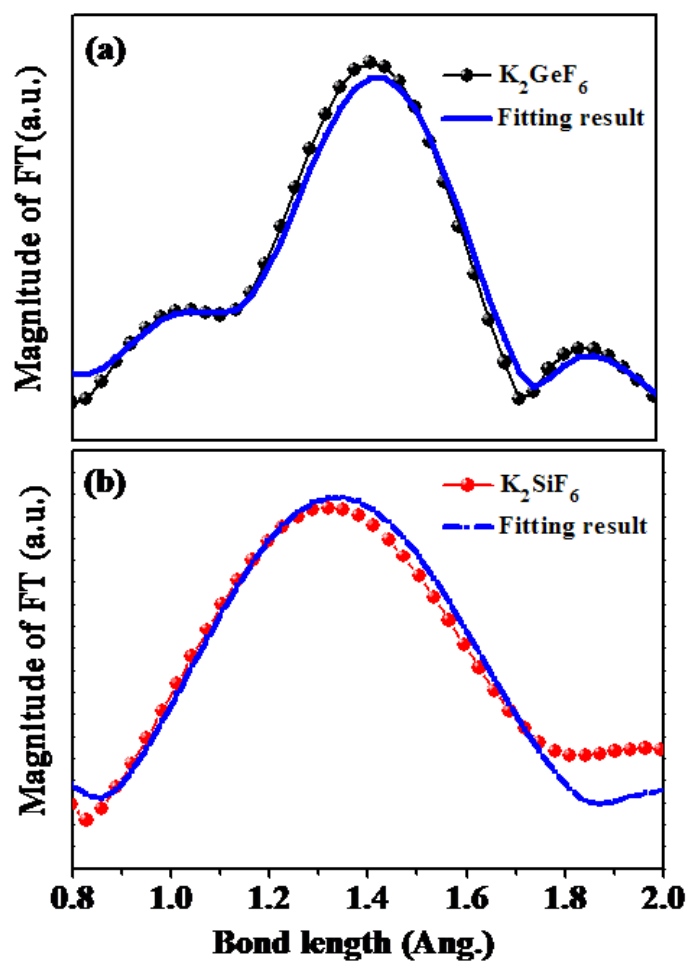


Figure S5. Fourier-transforms fitting of EXAFS analysis for the coordination environments of Ge^{4+} and Si^{4+} ions.

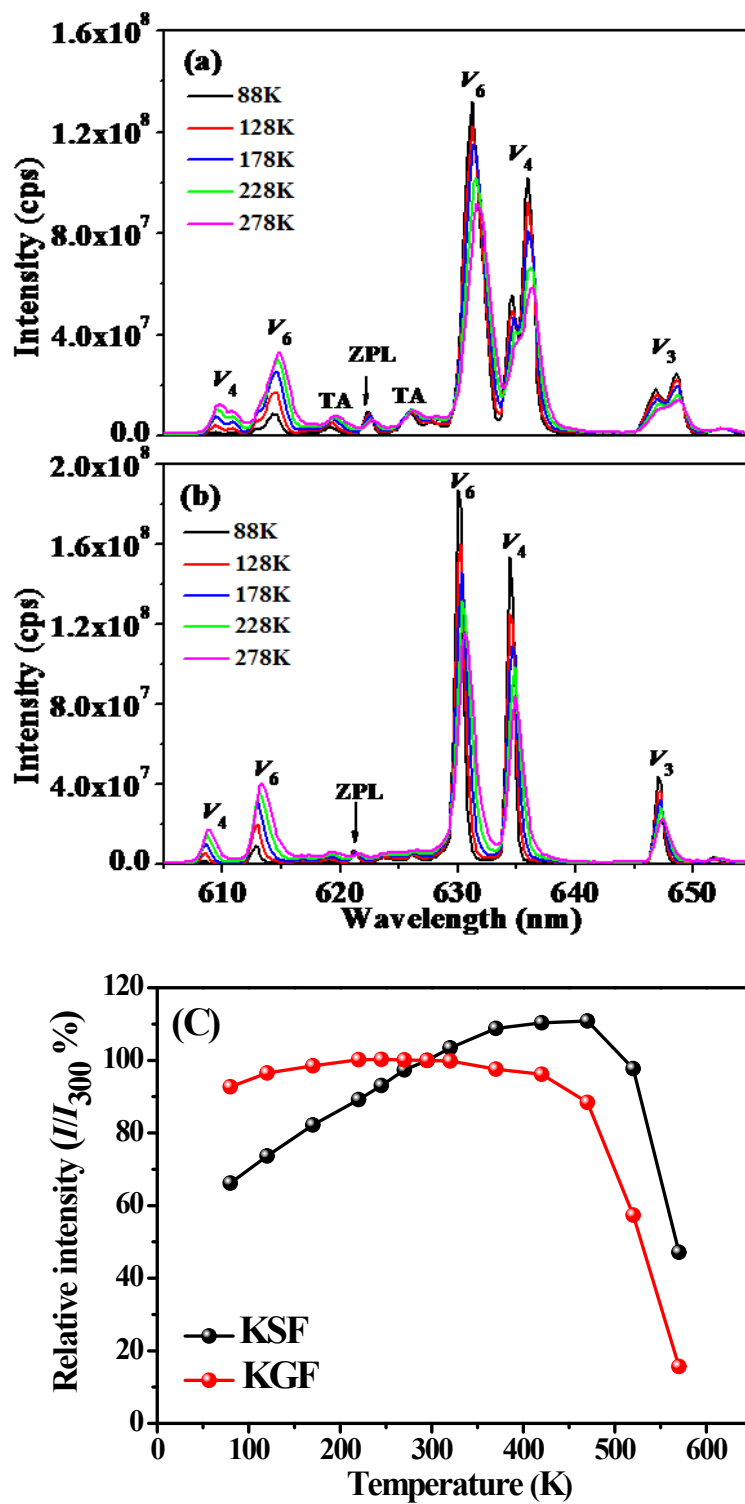


Figure S6. Temperature-dependent PL spectra of $\text{K}_2\text{GeF}_6:\text{Mn}^{4+}$ (a) and $\text{K}_2\text{SiF}_6:\text{Mn}^{4+}$ (b) red phosphors. (c) The relationship of intensity and temperature was measured between 80 K and 570 K.

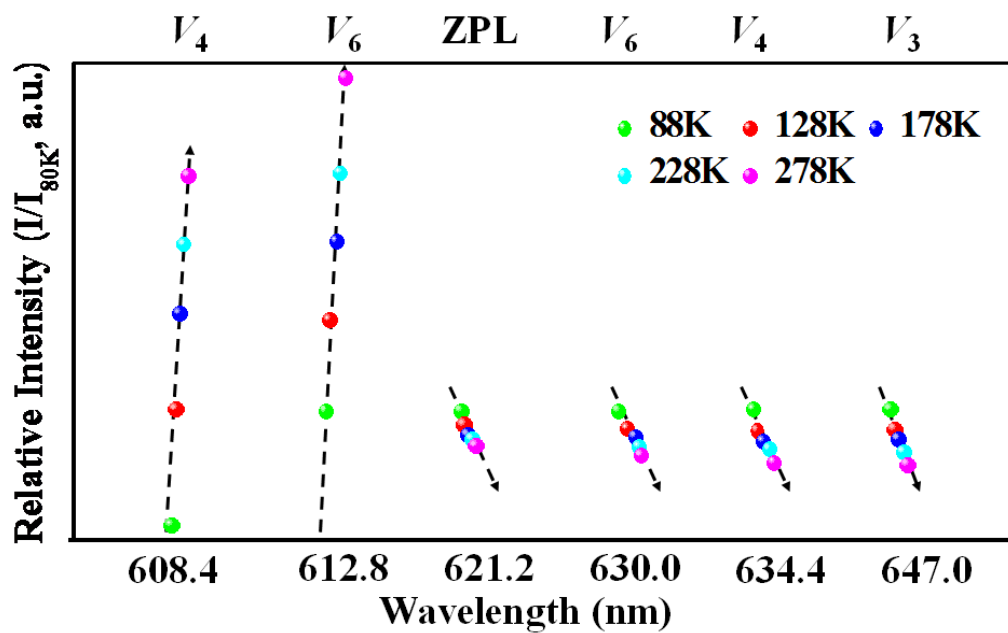


Figure S7. The wavelength position and relative intensity of each emission line obtained at different temperatures for $K_2SiF_6:Mn^{4+}$ red phosphor.

References:

- (1) B. Z. Malkin, A. A. Kaplyanskii and B. M. Macfarlane, *Spectroscopy of solids containing rare-earth ions*, Amsterdam: North-Holland, 1987; p. 13.
- (2) N. M. Avram and M. G. Brik, *Optical Properties of 3d-Ions in Crystals: Spectroscopy and Crystal Field Analysis*, Springer and Tsinghua University Press, 2013.
- (3) M. Kirm, G. Stryganyuk, S. Vielhauer, G. Zimmerer, V. N. Makhov, B. Z. Malkin, O. V. Solovyev, R. Y. Abdulsabirov and S. L. Korableva, *Phys. Rev. B.* 2007, **75**, 075111-1~13.
- (4) B. Z. Malkin, T. T. A. Lummen, P. H. M. Van Loosdrecht, G. Dhalenne and A. R. Zakirov, *J. Phys.: Condens. Matter.* 2010, **22**, 276003-1~11.
- (5) M. Vaida and C. N. Avram, *Acta Phys. Polonica A* 2009, **116**, 541-543.
- (6) A. M. Srivastava and M. G. Brik, *Opt. Mater.* 2013, **35**, 1544-1548.
- (7) R. M. Krsmanović Whiffen, D. J. Jovanović, Ž. Antić, B. Bártoová, D. Milivojević, M. D. Dramićanin and M. G. Brik, *J. Lumin.* 2014, **146**, 133-140.
- (8) S. J. Clark, M. D. Segall, C. J. Pickard, P. J. Hasnip, M. J. Probert, K. Refson and M. C. Payne, *Z. Kristallogr. NCS.* 2005, **220**, 567-568.
- (9) J. P. Perdew, K. Burke and M. Ernzerhof, *Phys. Rev. Lett.* 1996, **77**, 3865-3868.
- (10) D. M. Ceperley and B. J. Alder, *Phys. Rev. Lett.* 1980, **45**, 566-569.
- (11) J. P. Perdew and A. Zunger, *Phys. Rev. B.* 1981, **23**, 5048-5079.
- (12) M. G. Brik and A. M. Srivastava, *J. Electrochem. Soc.* 2012, **159**, J212-J216.